JOURNAL OF MATERIALS SCIENCE 26 (1991) 6135–6143

Processing and properties of superconducting $YBa_2Cu_3O_{7-x}$ powder by single-step calcining in air

J. TARTAJ, C. MOURE, P. DURAN
Instituto de Cerámica y Vidrio (CSIC), Electroceramics Department, Arganda del Rey, 28500 Madrid, Spain

J. L. GARCIA-FIERRO
Instituto de Catálisis y Petroquímica (CSIC), Serrano 115, 28006 Madrid, Spain

J. COLINO
Instituto de Ciencia de Materiales (Sede A), CSIC, Madrid, Spain

The preparation of orthorhombic $YBa_2Cu_3O_{7-x}$ powder using only one calcination step is described. Yttrium and copper nitrates and barium carbonate were used as precursor materials. The use of an appropriate precipitant agent leading to a complete coprecipitation of the Y^{3+} and Cu^{2+} cations, promoted the rapid low temperature formation of $YBa_2Cu_3O_{7-x}$ (900 °C for 4 h) with no secondary phases. X-ray diffraction patterns of the obtained powder showed the presence of the only one phase with the orthorhombic structure, and lattice parameters of $a = 0.3824$ nm, $b = 0.3893$ nm, $c = 1.1676$ nm and $\sigma = 1.775$ which correspond to a superconducting $YBa_2Cu_3O_{6.95}$ phase. Sintering compacted samples at 940 °C several times led to highly dense ($\geqslant$ 96% theoretical density) superconductor bodies, and a value of T_c as high as 94 K was measured. Although AES depth profiles in fracture surfaces evidenced good grain boundaries of the superconducting $YBa_2Cu_3O_{6.95}$ samples, however, the J_c measured was never greater than 15 A cm^{-2}, which could be due to a weak-link region between high J_c grains. Slow degradation of the $YBa_2Cu_3O_{6.95}$ ceramics seems to take place by the formation of $Ba(OH)_2$ and YO(OH) at the superconductor surface in contact with the moisture of the air.

1. Introduction

The most common route used for fabricating high T_c superconducting powders is the conventional solid-state reaction: $\frac{1}{2}Y_2O_3 + 2\,BaCO_3 + 3\,CuO \rightarrow YBa_2Cu_3O_{6.5} + CO_2$, in which no addition or depletion of oxygen during the calcination could be assumed. Such a synthesis process, however, presents many problems; the most important of which concerns barium carbonate decomposition. Its high decomposition temperature leads, in the majority of the cases, to an incomplete $YBa_2Cu_3O_{7-x}$ phase formation and very long reaction times would be necessary to enhance the barium carbonate decomposition. On the other hand, the presence of no decomposed barium carbonate could favour the reaction kinetics to form phases other than $YBa_2Cu_3O_{7-x}$ and, in some cases, the formation of a low temperature eutectic liquid from the $BaCO_3$–CuO binary system. The formation of a secondary phase or the eutectic liquid could impair the critical current density by diminishing the connectivity degree between the superconducting grains. The presence of either of them should, therefore, be avoided.

In order to reach better homogeneity which favours single-phase $YBa_2Cu_3O_{7-x}$ formation, wet-chemical techniques such as coprecipitation [1, 2], sol–gel [3] and freeze drying [4] have been recently used. The present paper was undertaken to prepare single-phase orthorhombic $YBa_2Cu_3O_{7-x}$ powder, in a single step calcining in air, by using a modified coprecipitation method.

2. Experimental procedure

High purity nitrate salts of copper and yttrium and barium carbonate were used as starting materials. The required amount of each nitrate salt was dissolved in bidistilled water, and then mixed together in a uniform solution by stirring. That nitrate solution was added by dropping on to an aqueous suspension containing the required amount of barium carbonate powder. A potassium hydroxide solution was used as precipitant agent by adding to the above described suspension, and a grey–black slurry was obtained at the end of the precipitation process. After filtering, the precipitate was thoroughly washed with distilled water to remove any potassium salts present. After washing, the powder was milled and washed again with distilled water. The powder was deagglomerated in a disc turbine, which, operating at 2000 r.p.m., provided a high liquid

0022–2461/91 $03.00 + .12

flow which enabled a maximum removal of water out of the agglomerated structure, and simultaneously a strong deagglomeration of the powder. Subsequently, the powder was calcined at 900 °C for 4 h in air and slowly cooled to room temperature. The calcined powder was deagglomerated again in a disc turbine at 7000 r.p.m., for 2 min, dried, isopressed at 200 MPa, and sintered at 940 °C several times in air. No additional oxygen annealing was carried out.

The particles size and morphologies of both the coprecipitated and the calcined powders were studied by SEM. On calcined powders and on sintered samples, the present phases were studied by X-ray diffraction, and the (2 0 0), (0 2 0) and ($\bar{0}$ 0 6) diffraction lines were taken into account to distinguish them. The reduced tetragonal phase and the completely oxidized orthorhombic one each show two diffraction lines but with reversed relative intensities. The splitting of the (0 2 0) and (2 0 0), and (1 2 3) and (2 1 3) peaks was taken into account to evaluate the orthorhombic distortion and, indirectly, the oxygen content of the orthorhombic $YBa_2Cu_3O_{7-x}$ phase.

On sintered samples the density was measured by the Archimedes method, and the microstructure was examined on polished samples by using an optical microscope and/or SEM. Elemental analysis was performed with an energy dispersive X-ray analyser (EDX) to identify the phases present in the sintered samples. Electrical resistance and critical current density at 77 K under zero applied magnetic field were measured using the four-probe technique.

The Auger measurements were performed in a Scanning Auger Microprobe (Jeol Jamp-105) with the following working conditions: 10 keV of energy for the primary electrons beam with a 0.1 mm diameter indice zone on the sample, and typical electronic currents of 500 nA. The ion milling for depth analysis was provided by an Ar^+ ion beam of 3 keV and 20 nA on a rastered area of 0.5×1 mm^2. The equivalent sputter rate was 3 to 5 A min^{-1} as described from a calibration on a $YBa_2Cu_3O_{7-x}$ thin film. This rate is employed in Fig. 9 for the estimated depth of the x axis.

Surface analysis of air-degraded $YBa_2Cu_3O_{7-x}$ samples was performed by X-ray photoelectron spectroscopy. Four samples labelled 1, 2, 3 and 4, which had been exposed for several days to air were studied and, for comparison the obtained results on the same samples subsequently oxidized at 400 °C in dry CO_2 free air, and vacuum degasified at 110 °C. The XPS spectra for the two kinds of samples were obtained by using an electron spectrometer in the working conditions described elsewhere [5].

3. Experimental results

3.1. Powder characterization

Fig. 1 shows that coprecipitated powder was constituted by a mixture of barium carbonate platelets (2×0.5 μm^2 average), and an amorphous agglomerated powder of small particles (50 nm). After 4 h calcination at 900 °C, the coprecipitated powder was converted into the 1–2–3 orthorhombic phase as shown in

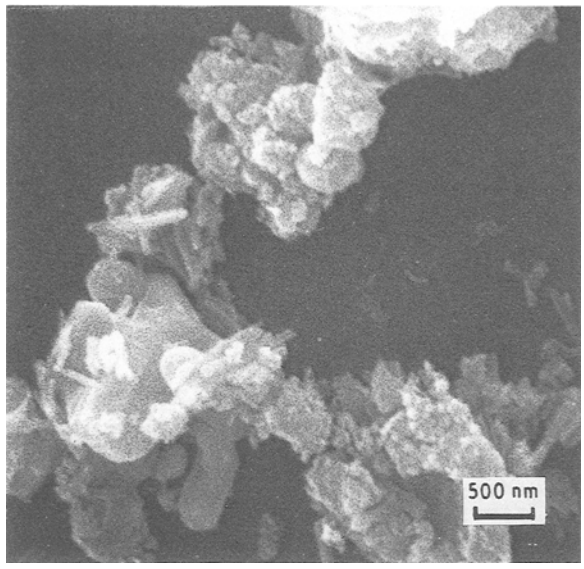

Figure 1 Scanning electron micrograph of coprecipitated powder.

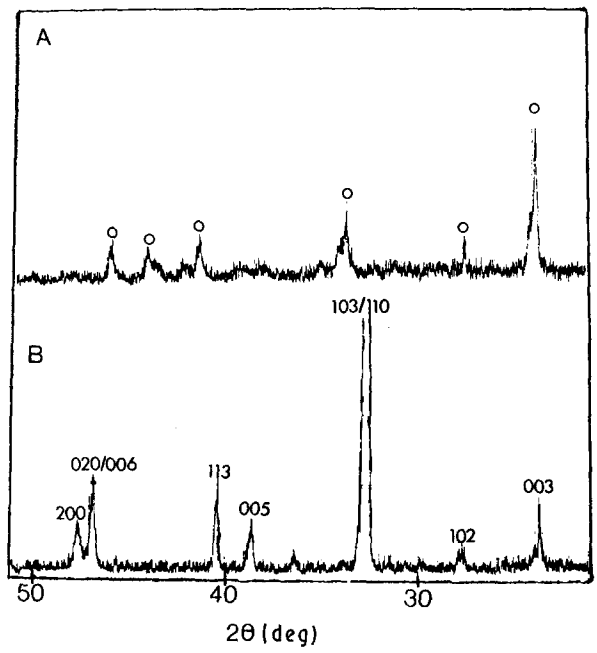

Figure 2 XRD patterns of (a) coprecipitated powder, and (b) calcined powder.

Fig. 2, and no minor phases were detected by XRD. The calcined powder was formed by porous soft agglomerates (40 to 60 μm size), see Fig. 3a, which during the slow cooling allowed an easy oxygen diffusion into the powder. The lattice parameters of the calcined powder were: $a = 0.3825 \pm 0.0005$ nm, $b = 0.3891 \pm 0.0005$ nm, and $c = 1.167 \pm 0.0005$ nm, which correspond to a well oxygenated $YBa_2Cu_3O_x$ ($x = 6.95$) orthorhombic phase.

Chemical analysis of the calcined powder revealed the presence of a residual 0.005 wt % K_2O with no significant influence on the 1–2–3 phase structure. Fig. 3b shows in detail the microstructure of the porous agglomerates which were formed by interconnected small grains (1 to 2 μm). By comparison with the normally exaggerated grain growth present in $YBa_2Cu_3O_{7-x}$ ceramics, it could be said that the K_2O

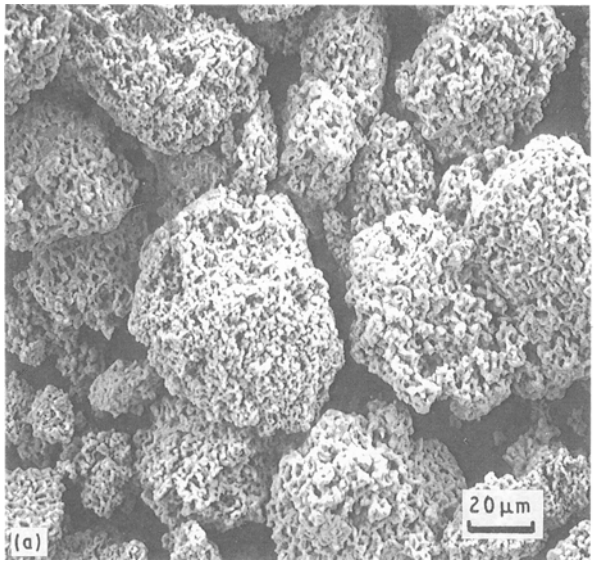

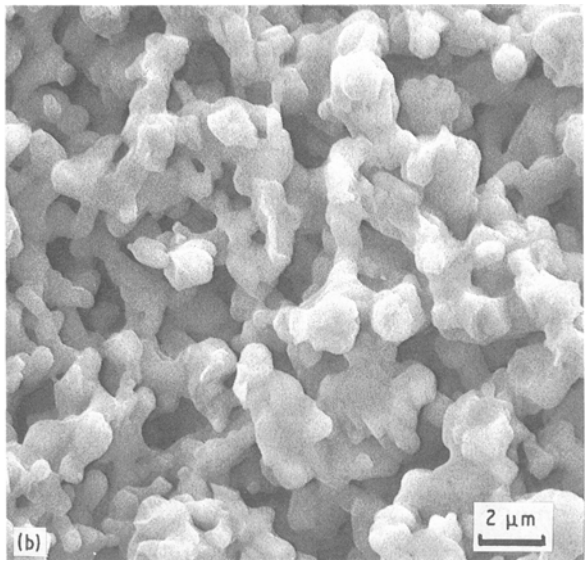

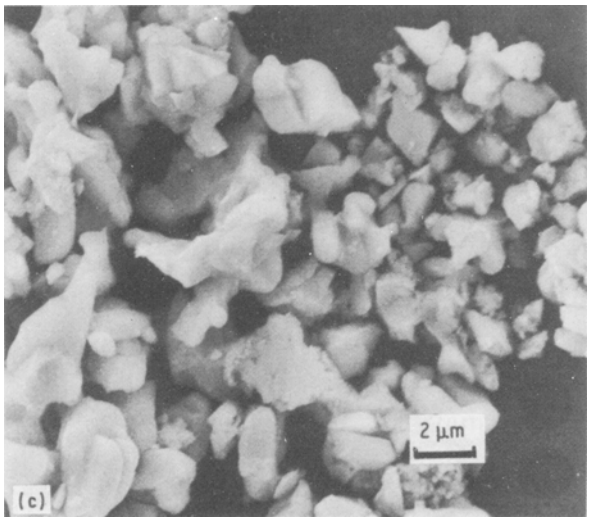

Figure 3 SEM of (a) porous calcined powder, (b) details of the porous agglomerated microstructure and (c) porous agglomerates after milling.

impurity acts as a grain growth inhibitor. On milling, the size of the agglomerates was reduced to about 1 to 2 µm, see Fig. 3c.

3.2. Sintering and microstructure

In order to avoid the formation of an eutectic liquid [6, 7] during the densification process, the samples were sintered at 940 °C. The effect of the sintering time on the compacts is shown in Fig. 4. The samples sintered for 2 h were 98% of the theoretical density ($D_T = 6.39\ g\ cm^{-3}$), and for longer sintering times the density decreased to about 95 to 96%.

It must be mentioned that the highly densified samples did not allow good oxygenation during the cooling, and most of them did not show superconductivity. The lattice parameters of a sample thus sintered for 2 h typically were: $a = b = 0.3883 \pm 0.0005$ nm and $c = 1.1685 \pm 0.0005$ nm, corresponding to a well defined tetragonal $YBa_2Cu_3O_{7-x}$ phase. All the samples sintered in air for 4 and 8 h at 940 °C showed a well defined orthorhombic $YBa_2Cu_3O_{7-x}$ superconducting phase, where x varied between 6.88 and 6.98 and the a and b lattice parameters, as shown in Fig. 5, hardly varied in that oxygen content range. On

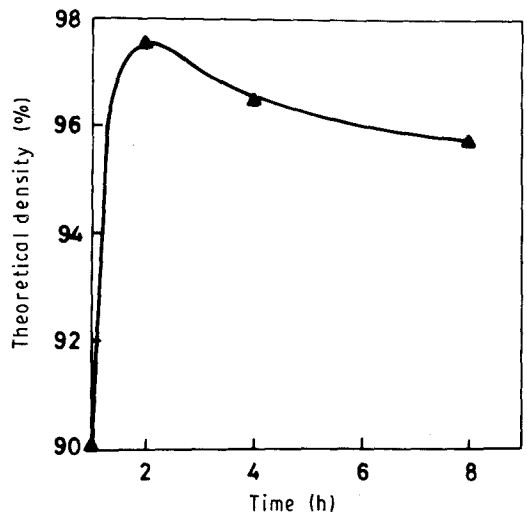

Figure 4 Sintering process plotted against time of the $YBa_2Cu_3O_{7-x}$ compacted samples. Sintering temperature 940 °C.

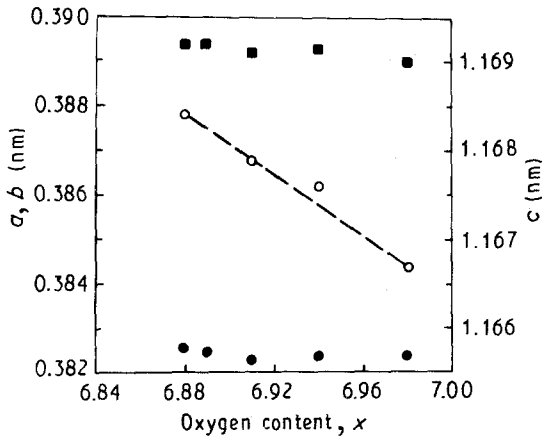

Figure 5 Lattice parameters variation of $YBa_2Cu_3O_{7-x}$ samples plotted against oxygen content. (● a, ■ b, ○ c).

the contrary, the variation of the parameter c was considerable. A typical set of lattice parameters of a superconducting sample was $a = 0.3825 \pm 0.0005$ nm, $b = 0.3894 \pm 0.0005$ nm and $c = 1.1683 \pm 0.0005$ nm.

Microstructure of the higher densified samples, Fig. 6a, showed elongated grains without any twinning which is typical of a non-superconducting material. The appearance of large-scale twinning in the samples less densified, Fig. 6b and c, is a consequence of the tetragonal to orthorhombic transformation which takes place on cooling from the sintering temperature. Such a twinning phenomenon is omnipresent in the microstructure of $YBa_2Cu_3O_{7-x}$ superconductor ceramics, and it is closely related to the direction of ordering of oxygen vacancies within the basal plane. It could be assumed that the broad faces corresponded to the platelets parallel to the basal plane. The residual porosity located, in some cases, in the interior of the platelets indicates that these have grown very rapidly, and no second phases were detected. The microstructure of these samples was also examined by SEM. Fig. 7 shows that all the superconducting $YBa_2Cu_3O_{7-x}$ grain boundaries contain a thin layer of an unknown secondary phase. Fig. 8 shows the EDX spectra of the phases present in the thin layer and that corresponding to a $YBa_2Cu_3O_{7-x}$ grain. EDX analysis indicates that the thin layer contained mainly Ba and Cu. Y was not present. This result could indicate that a eutectic liquid, probably from the $BaCO_3$–CuO system, was formed at low temperature during the calcination and remained throughout the sintering process. Guha [8] reported that the formation of a eutectic liquid at low temperature was very difficult to avoid, however, he attributed the presence of a liquid along the grain boundaries to be formed from the ternary system $YBa_2Cu_3O_{7-x}$–$BaCuO_2$–CuO. The non CuO_x enrichment of the grain boundaries, see below, and the absence of Y in the EDX analysis of the liquid film, (Fig. 8), lead to assume that such a liquid could be a binary eutectic one from the $BaCO_3$–CuO system, and that the amount of CuO in the same was very small.

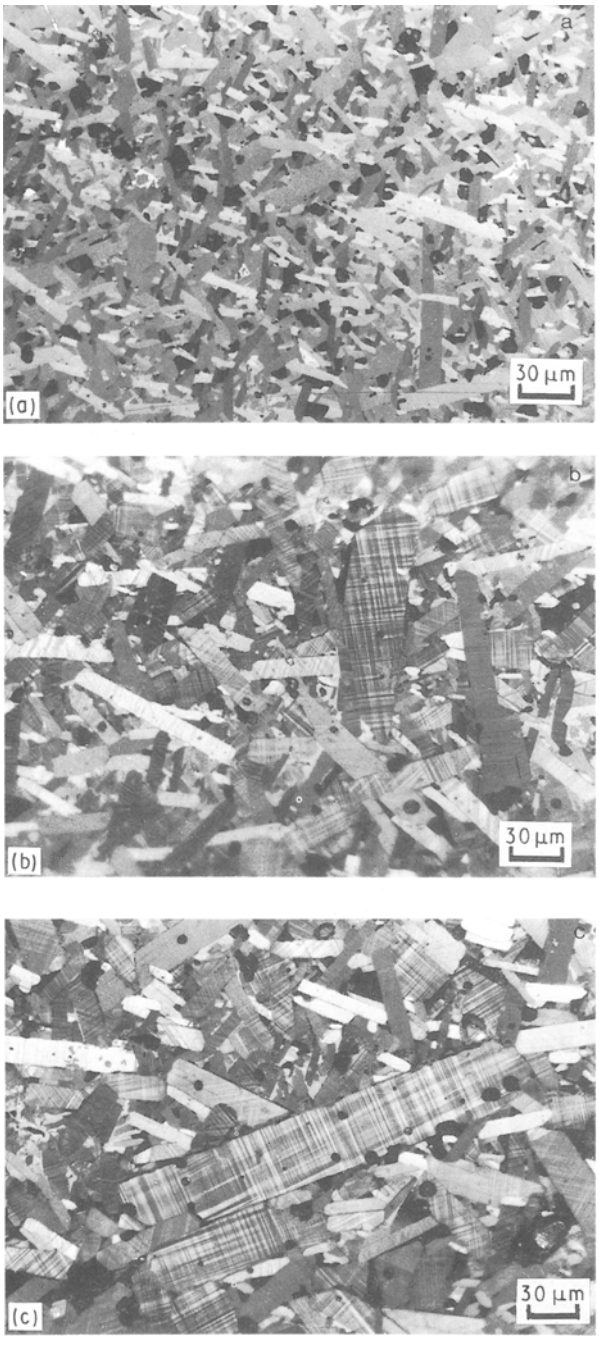

Figure 6 Polarized optical micrographs of $YBa_2Cu_3O_{7-x}$ samples sintered at 940 °C for (a) 2 h, (b) 4 h and (c) 8 h.

3.3. Auger electron spectroscopy

AES depth profiles in fracture surfaces of conventional $YBa_2Cu_3O_x$ ceramics have been extensively studied taking into account the ion beam effects [9]. One of the main conclusions obtained there was the synthesis of a pressed $YBa_2Cu_3O_x$ powder disc which produces a copper-enriched surface layer at the grain boundaries, so that the formation of these weak links are an additional cause for J_c depletion.

For the superconducting $YBa_2Cu_3O_x$ ceramics studied here, the depth profile of the fracture surfaces is presented in Fig. 9. The value of the intensity for each element was determined from the peak-to-peak

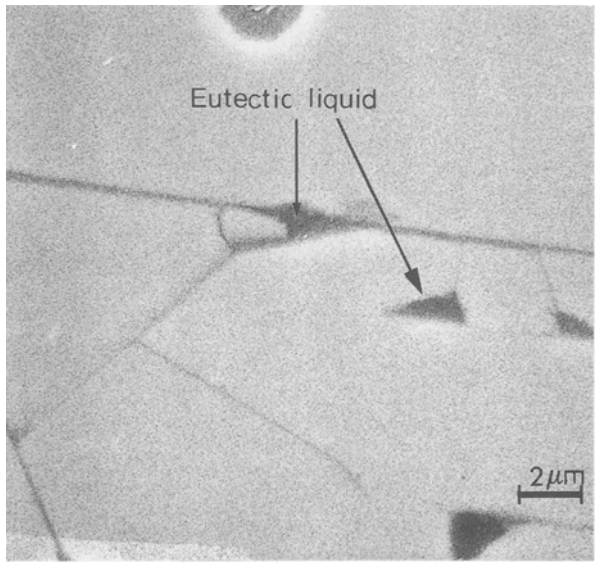

Figure 7 SEM of $YBa_2Cu_3O_{7-x}$ sintered samples showing grain boundaries liquid thin layer.

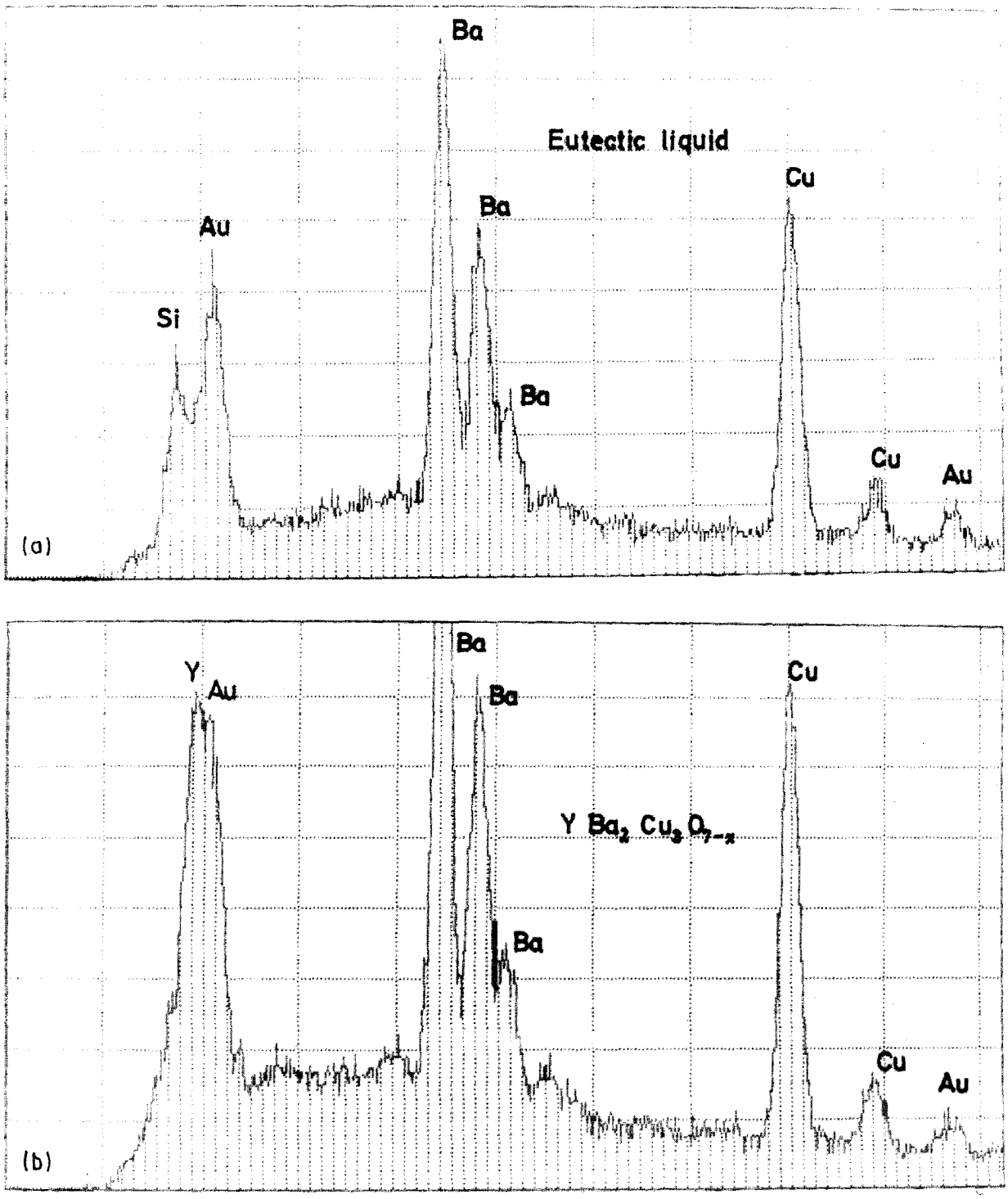

Figure 8 EDX spectra of (a) liquid thin layer, and (b) $YBa_2Cu_3O_{7-x}$ grains.

intensity in the Auger spectra ($dN(E)/dE$ plotted against E). Peaks employed are: C KLL 272 eV, O KLL 519 eV, Ba MNN 594 eV, Cu LMM 926 eV and Y LMM 1765 eV. The measured profiles have been normalized to the Auger intensity of the barium, so that variations of the I_x/I_{Ba} ratio are similar to the variations of the ratio of concentrations. The estimated depth was calculated as described above.

The main effect of the ion bombardment (Ar^+ 3 keV in our case) is an expected apparent oxygen surface enrichment, as in simple oxides, and other slight changes for the metallic elements [9]. First it is important to note that, as in other $YBa_2Cu_3O_x$ surfaces [9], no apparent oxygen-rich surface layer is observed here, which suggests a spontaneous oxygen release. This effect was reported in the same structure by photoemission experiments [10], where the room temperature activation was the assumed mechanism. On the other hand, the profiles of metallic ratios rather agree with the expected behaviour for a homogeneous sample [9], so that no significant variations of metallic elements occur at the fracture surface. The measured profiles are a proof of good grain boundaries in these samples. The CuO_x segregation at grain boundaries for conventional ceramics has been avoided. No potassium signal was detected either at the fracture surface or at the surface bombardment due to its low concentration.

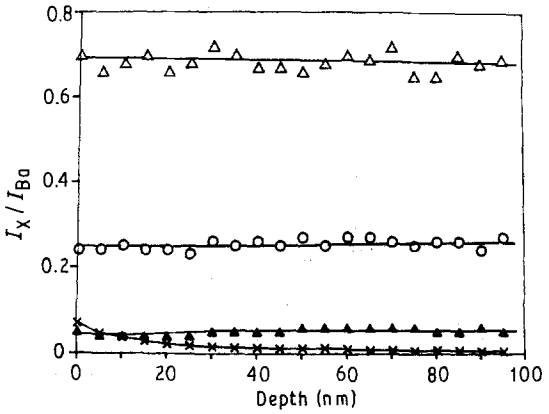

Figure 9 AES depth profiles on $YBa_2Cu_3O_{7-x}$ fracture surface samples. (△Ox/Ba/10, ○ Cu/Ba, ▲ Y/Ba, × C/Ba/10).

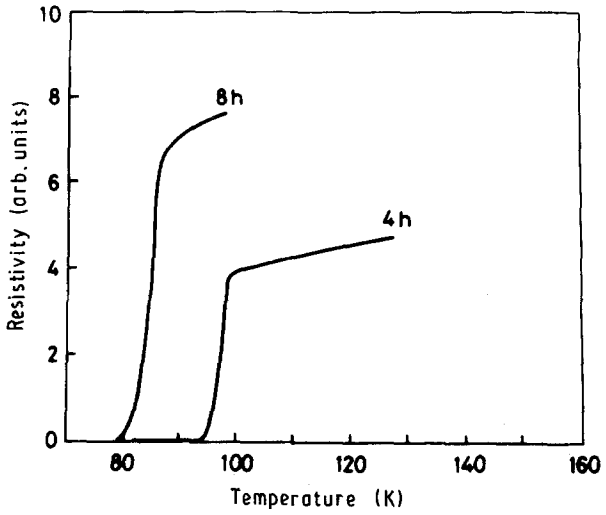

Figure 10 Resistivity temperature curves for $YBa_2Cu_3O_{7-x}$ samples with different oxygen content.

3.4. Superconducting properties

Since the superconducting characteristics strongly depend on the grain boundaries, resistivity measurements were performed for all samples at a sample current of 10 mA, and at temperatures above the liquid nitrogen temperature. Typical resistivity curves are shown in Fig. 10, for samples sintered at different times. As expected, the sample with a lower oxygen content (8 h) showed a curve in which the resistivity decreases slowly with decreasing temperature. The onset temperature was about 89 K, and the zero-resistivity temperature was approximately 80 K. In the case of the higher oxygen content sample (4 h), the resistivity drops sharply near the zero-resistivity temperature. The superconducting onset temperature and the zero-resistivity one were about 96 and 94 K, respectively.

Although the samples were highly densified, J_c was, however, never higher than 15 A cm^{-2}, and in some cases dramatically decreased to about 1 A cm^{-2}. The presence of very small amounts of undetected second phases, was probably responsible for these low J_c values.

3.5. Photoelectron spectroscopy study

As described above, the surface analysis was performed on four superconducting $YBa_2Cu_3O_{7-x}$ samples labelled 1, 2, 3 and 4 which had been exposed to the moisture of the ambient atmosphere at room temperature. Then the same samples were oxidized at 400 °C in CO_2 free air, and finally the samples were vacuum degasified at 110 °C. Fig. 11a and b shows the XPS spectra of O 1s before and after the oxidation heat treatment. In general, the spectra of the non-oxidized samples are quite broad, except for sample 3, in which a majority contribution to BE in the range of 530.8 to 531.4 eV could be observed. An overlapped second peak at higher BE_s was also detected. After oxidation and subsequent degasification noteworthy changes took place (see Fig. 11b). The overlapped peak at higher BE_s disappears, and another one in the region of 529.5 to 530.1 eV appears. The peak at about 531 eV, only present in the samples exposed to moisture, is still a majority contribution in the sample 3, decreases in samples 2 and 4, and was very small in sample 1. According to these spectra peculiarities, the peak at about 529.6 eV can be assigned to O^{2-} ions, and the peak at higher BE (531.0 eV) is typical of less electron-rich oxygen species, i.e. hydroxyl groups. The highest BE peak is characteristic of absorbed water molecules.

The XPS spectra Ba $3d_{5/2}$ of the samples exposed to moisture and those obtained after the oxidation–degasification process are shown in Fig. 12a and b. Two well defined peaks at 779.8 and 781.3 eV for the moisture-exposed samples were observed. In the case of sample 3, only one peak, at 779.5 eV, was detected. After degasifying the Ba $3d_{5/2}$ line profile presents some important changes in comparison to that obtained on the moisture exposed samples. As shown in Fig. 12b, the highest BE peak disappeared and another one at 780.0 eV is present.

The existence of two peaks in the Ba $3d_{5/2}$ level for the moisture-exposed samples indicates the presence of two Ba^{2+} species. The higher BE peak is characteristic of Ba^{2+} ions in an environment of O^{2-} ions. The lower BE peak corresponds, therefore, to $Ba(OH)_2$ hydroxide species. The way these hydroxide species disappeared after the oxidation–degasification treatment indicates that the formed surface $Ba(OH)_2$, quantitatively decomposed. Such a result is contradictory to that found in the XPS spectra O 1s of the moisture-exposed and subsequently degasified samples in which OH^- groups were detected. Such apparent inconsistency can be explained by the fact that the remnant OH^- groups are not associated to the Ba^{2+} ions but the Y^{3+} ions (see below).

The XPS spectra corresponding to the Cu $2p_{3/2}$ level are shown in Fig. 13a and b. All of them present the Cu $2p_{3/2}$ level and the corresponding satellite lines at the higher BE with the characteristics of the Cu^{2+} ions. All the moisture-exposed samples show the Cu $2p_{3/2}$ level quite enlarged and the corresponding satellite lines are poorly defined. It must be mentioned that the binding energy is about 1 eV higher than the Cu $2p_{3/2}$ level of the oxidized samples. This result seems, in principle, contradictory since the oxidized

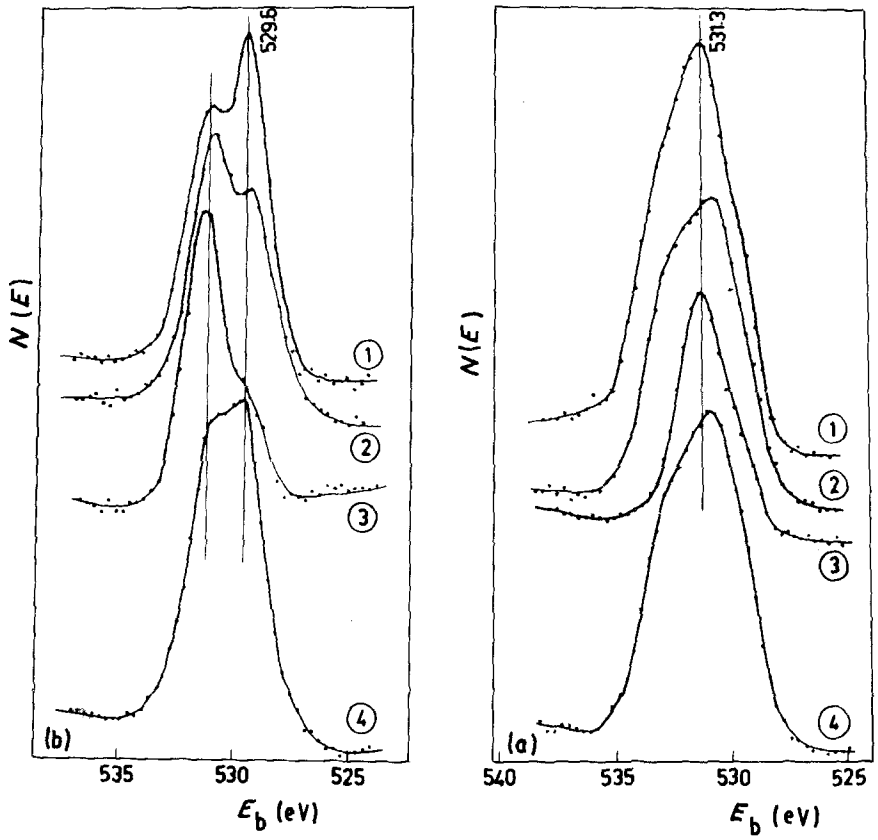

Figure 11 XPS photoemission lines of O 1s in $YBa_2Cu_3O_{7-x}$ samples (a) before and (b) after oxidation heat treatment.

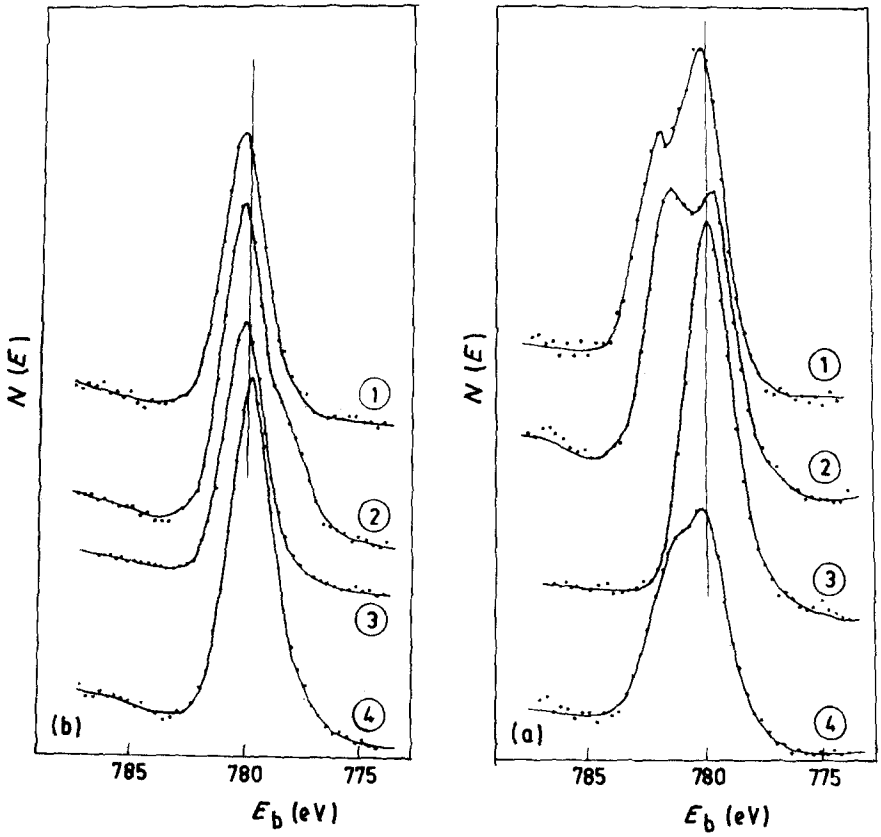

Figure 12 XPS spectra Ba $3d_{5/2}$ of (a) samples exposed to moisture and (b) after the oxidation–degasification treatment.

samples should have copper species of the Cu^{3+} type which imply a higher BE for the Cu $2p_{3/2}$ level. This could indicate the presence of a high OH^- groups concentration in the vicinity of the Cu^{+2} ions and, probably, carbonate species too. This last assumption is based on the fact of the appearance of some amounts of CO_3^{2-} species in all the samples and especially in sample 3. Both of the OH^- groups and the

TABLE I Binding energies (eV) of several $YBa_2Cu_3O_{7-x}$ samples

Sample	C 1s		O 1s		Cu $2p_{3/2}$	Ba $3d_{5/2}$	Y $3d_{5/2}$	
1		969.5		722.8	320.0	473.9		1096.2
				531.3	934.1	780.2		157.9
2		969.3		723.1	319.5	474.4	1096.7	1097.6
				530.8	934.4	779.5	157.2	156.3
3	964.2	969.5		717.4	315.3	468.9		1091.9
				531.4	933.5	779.9		156.9
4		969.5		723.2	319.7	474.3		1098.1
				530.9	934.4	779.8		156.0
1 oxi (deg)		969.4		724.4	321.1	473.8		1098.1
				529.6	932.9	780.2		155.9
2 oxi (deg)		969.5		724.6	321.5	473.9		1097.8
				529.5	932.6	780.2		156.3
3 oxi (deg)	962.5	969.3	716.2	717.0	314.0	467.0		1091.0
			530.9	530.1	933.1	780.1		156.1
4 oxi (deg)		969.3		724.1	321.2	474.1		1097.9
				529.8	932.7	779.8		156.0

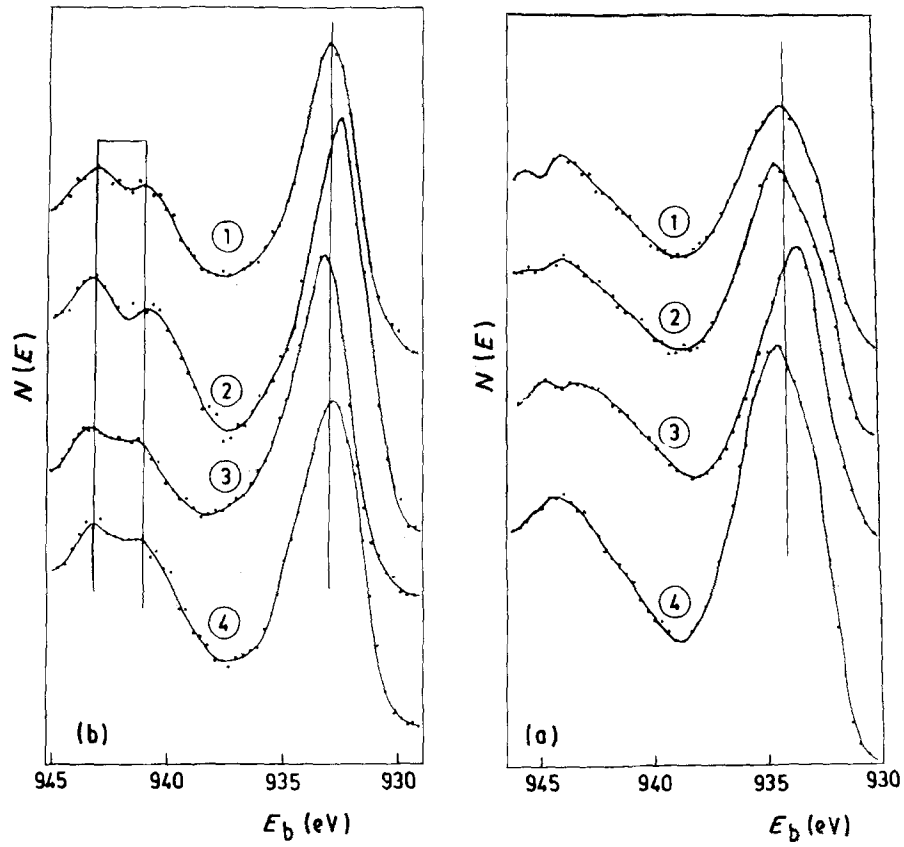

Figure 13 XPS spectra Cu $2p_{3/2}$ of $YBa_2Cu_3O_{7-x}$ samples (a) before and (b) after oxidation–degasification treatment.

CO_3^{2-} species are decomposed and almost eliminated during the oxidation–degasification treatment, and some remnant OH^- groups remain on the surface sample associate to the Y^{3+} ions giving rise to the formation of very stable oxo-hydroxide species YO(OH).

To get an insight of the present phases on the surface of the oxidized samples the superficial atomic ratios were calculated. These ratios are summarized in Table I. In this calculation normalized intensities for Cu $2p_{3/2}$, Ba $3d_{5/2}$ and Y $3d_{5/2}$ levels and published sensitivity factors have been considered. From the data of Table I it can be observed that these atomic ratios are far from those corresponding to a stoichiometric $YBa_2Cu_3O_{7-x}$. The Cu to Y atomic ratio is about a half to a third smaller than the theoretical value. The Ba to Y atomic ratio is, however, reasonably good. It must also be mentioned that for the O to Y + Ba + Cu atomic ratio, the theoretical value of 1.17, changes from 1.23 in sample 1 to 2.40 in sample 4. All these facts indicate that during the exposition of the samples to the ambient moisture at room temperature a thin film of $Ba(OH)_2$, YO(OH) and small amounts of carbonates in the layer immediately below the external surface sample was formed. The subsequent oxidation treatment does not regenerate in that surface region the stoichiometric $YBa_2Cu_3O_{7-x}$ structure.

4. Discussion

The use of KOH as a precipitant agent seems to lead to a stoichiometric precipitation of the Y^{3+} and Cu^{2+} cations in processing a nitrate salts mixture in the presence of $BaCO_3$. Such an intimate powder mixture ($Y(OH)_3$ + $Cu(OH)_2$ + $BaCO_3$) led to the formation of a well defined orthorhombic $YBa_2Cu_3O_{7-x}$ single phase by calcining at 900 °C for 4 h in air, and no second phases were present. It is believed that the presence of a small amount of residual KOH favoured the decomposition of $BaCO_3$ at lower temperature, leading to the formation of $YBa_2Cu_3O_{7-x}$ as the only reaction product during the calcination. Two main factors seem to favour the formation of a superconducting $YBa_2Cu_3O_{7-x}$ phase during the cooling, (a) the formation of porous agglomerates which facilitate the oxygen diffusion into the powder and (b) the probable increasing of T–O transition temperature [1] by the presence of K^+ ions leading to faster oxygenation kinetics.

In sintered $YBa_2Cu_3O_{7-x}$ samples the tetragonal to orthorhombic conversion was not completed in those highly densified owing to the difficulty for the oxygen diffusion into the pellets. More porous samples were completely converted to fully orthorhombic $YBa_2Cu_3O_{7-x}$ during the cooling in air, which indicates a better oxidation behaviour. In that way, O'Bryan and Gallagher [11] found that the oxidation of porous pellets was 90% complete in 0.5 h at 700 °C. It seems that the existence of some open porosity was necessary for achieving both good oxidation and low microcracking. The pores could be acting to arrest crack propagation.

As expected (see Fig. 10) the more oxygenated samples showed a higher T_c, coinciding with the largest orthorhombic distortion. Their lattice parameters closely converged to those of $YBa_2Cu_3O_{7-x}$, and a heavily twinned microstructure of the (1 1 0) type was observed. No good correlation between microstructure and resistive behaviour was found, and thus low values of J_c (1 to 15 A cm^{-2}) were always measured on the samples despite the well defined superconducting phase and good microstructural development. It could be due, in principle, to a poor mechanical contact between the surface grains or to a different nature of the weak link [12]. Such an assumption would, however, be contradictory to a homogeneous metal distribution as above found by the Auger spectroscopy technique. It could then be assumed that the detected thin liquid film located at the grain boundaries, (see Fig. 7), would be responsible for the low J_c values, or, if, as shown in Fig. 6b and c, the twin boundaries have a random orientation within the microstructure, then the low J_c values attained could also be a consequence of a high J_c anisotropy between the basal plane of the $YBa_2Cu_3O_{7-x}$ grains and the c direction. In that way, an enhancement of J_c could be achieved by producing the desired orientation in a controlled texture.

From the XPS experiments it was evidenced the relatively high reactivity of the $YBa_2Cu_3O_{7-x}$ superconducting material with water vapour from the air. Its degradation seems to take place by the formation of $Ba(OH)_2$ giving rise to the appearance of the corresponding amounts of Y_2O_3 and CuO free oxides, which subsequently react with water vapour to give yttrium oxo-hydroxide YO(OH) and some $CuCO_3$.

Acknowledgements

The authors wish to thank J. L. Sacedón for valuable discussions. This work was supported by the CICYT under project No. MAT88-0219 and by a grant from Rio Ródano, S. A.

References

1. I. W. CHEN, S. KEATING, C. Y. KEATING, X. WU, J. XU, P. E. REYES-MORRELL and T. Y. TIEN, *Adv. Ceram. Mater.* **2** (1987) 457.
2. C. MOURE, P. DURÁN, S. VIERA, S. BOURGEAL, R. VILLAR, A. AGUILO and M. RAMOS, British Ceramics Proceedings 40, "Superconducting Ceramics", edited by R. Freer (Institute of Ceramics, Shelton, Stoke-on-Trent, UK, 1988).
3. C. T. CHU and B. DUNN, *J. Amer. Ceram. Soc.* **70** (1987) C-375.
4. S. M. JOHNSON, M. I. GUSMAN, D. J. ROWCLIFFE, T. H. GEBALLE and J. Z. SUN, *Adv. Ceram. Mater.* **2** (1987) 337.
5. M. T. HERNANDEZ, J. R. JURADO, P. DURÁN and J. L. FIERRO, *J. Amer. Ceram. Soc.* **74** (1991) 1254.
6. K. G. FRASE and D. R. CLARKE, *Adv. Ceram. Mater.* **2** (1987) 295.
7. K. G. FRASE, E. G. LINIGER and D. R. CLARKE, *J. Amer. Ceram. Soc.* **70** (1987) C-204.
8. J. P. GUHA, *ibid.* **71** (1988) C-273.
9. J. COLINO, J. L. SACEDÓN, L. del OLMO and J. L. VICENT, *J. Vac. Sci. Technol A.* **8(6)** (1990) 4021.
10. R. S. LIST, A. J. ARKO, Z. FISK, S-W-CHEONG, S. D. CONRADSON, J. D. THOMPSON, C. B. PIERCE, D. E. PETERSON, R. J. BARTLETT, N. D. SLIMN, J. E. SCHIRBER, B. W. VEAL, A. P. PAULIKAS and J. C. CAMPUZANO, *Phys. Rev. B* **38** (1988) 11996.
11. H. M. O'BRYAN and P. K. GALLAGHER, *Adv. Ceram. Mater.* **2** (1987) 640.
12. J. W. EKIN, *ibid.* **2** (1987) 586.

Received 1 August 1990
and accepted 12 February 1991